Sea Clutter Suppression Based on Complex-Valued Neural Networks Optimized by PSD

Hongling Zhu, Ze Yu, *Member, IEEE*, and Jindong Yu

***Abstract*—Sea clutter suppression plays an important role in improving the estimation accuracy of the motion parameters of moving ships. Based on the chaotic characteristics of sea clutter, a novel sea clutter suppression method based on complex-valued neural networks optimized by power spectral density is proposed. The complex-valued neural networks helped reduce the phase prediction error of sea clutter, so that the sea clutter prediction accuracy was significantly improved compared with that of real-valued neural networks. The power spectral density function was added to the loss function of the complex-valued neural networks to optimize the training of the networks, and the prediction accuracy was further improved. The sea clutter could be effectively suppressed by cancellation and the signal-to-clutter ratio of the echo was improved. Experimental results based on measured sea clutter data validated the proposed method.**

***Index Terms*—Complex-valued neural networks, power spectral density (PSD), sea clutter suppression.**

I. Introduction

SEA clutter is the backscattered signal from the sea surface received by radar. Sea clutter makes it difficult to estimate the motion parameters of moving ships, resulting in the defocused images of targets [1]. Therefore, sea clutter suppression plays an important role in improving the image quality of sea–surface targets. This article proposes a novel sea clutter suppression method based on complex-valued neural networks optimized by the power spectral density (PSD).

At present, the sea clutter suppression methods mainly include the circulation cancellation, wavelet transform, subspace decomposition, and neural-network-based methods. The cancellation method constructs sinusoidal signals, estimates parameters based on the measured sea clutter, and then subtracts the sinusoidal signals from the echo to eliminate the sea clutter [2]. The wavelet transform method takes advantage of the differences between the sea clutter signal and the target signal in the wavelet domain and removes sea clutter by means of threshold segmentation [3]. The subspace decomposition method is based on eigenvalue decomposition or singular value decomposition. Sea clutter is separated from radar echo based on the clustering characteristics of clutter in the subspace [4], [5]. Neural-network-based methods are based on the chaotic characteristics of sea clutter [6]. The inherent chaotic dynamical characteristics of sea clutter can be learned to predict and suppress the sea clutter accurately. Based on a chaotic prediction theorem [7], [8], Haykin and Li [6] proposed a nonlinear prediction equation of sea clutter. The strong nonlinear fitting capability of neural networks provides great convenience for sea clutter prediction and suppression. Radial basis function neural networks and wavelet neural networks have been used to model nonlinear chaotic dynamical systems and predict sea clutter data [9], [10]. The improved general regression neural network algorithm was proposed to improve the prediction accuracy of sea clutter [11]. Compared with these static neural networks, long short-term memory (LSTM) neural networks possess a memory cell that can record the historical information and are more suitable for learning the long-term chaotic dynamical laws of sea clutter [12]. These neural networks are based on real-valued inputs, outputs, and weight factors, so the applications have been limited to real-valued data. These are called real-valued neural networks.

The received radar sea clutter is complex-valued signal after orthogonal modulation. Complex-valued sea clutter sequences are divided into real and imaginary parts and then processed separately by real-valued neural networks [13]. The processing procedure is complicated and the phase feature between the real and imaginary parts is ignored. The applications of complex-valued neural networks have expanded considerably in recent years [14], [15], [16], particularly in coherent radar systems. Complex-valued convolutional neural networks (CNNs) have been used for radar imaging, making the radar echo process more efficient [17]. Due to the richer representational capacity of complex-valued data, complex-valued neural networks show stronger generalization abilities than real-valued neural networks [18].

This article introduces a sea clutter suppression method based on complex-valued neural networks. In order to further improve the prediction accuracy of sea clutter, the PSD was utilized to optimize the complex-valued neural networks. Furthermore, sea clutter suppression was achieved based on sea clutter cancellation.

The rest of this article is organized as follows. Section II modifies the sea clutter prediction model from real-valued neural networks to complex-valued neural networks, and the PSD was used to optimize the complex-valued neural networks. Then, in Section III, a sea clutter suppression method based on the

Manuscript received 29 July 2022; revised 24 September 2022; accepted 26 October 2022. Date of publication 31 October 2022; date of current version 21 November 2022. This work was supported by the National Natural Science Foundation of China under Grant 62271031. *(Corresponding author: Jindong Yu.)*

The authors are with the School of Electronics and Information Engineering, Beihang Univeristy, Beijing 100191, China (e-mail: zhuhongling@buaa.edu.cn; yz613@buaa.edu.cn; yujindong92@buaa.edu.cn).

Digital Object Identifier 10.1109/JSTARS.2022.3218055

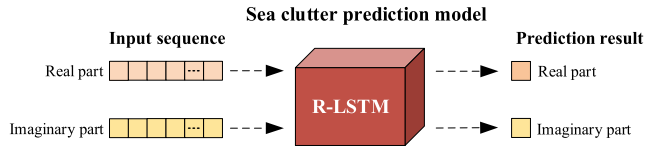

Fig. 1. Sea clutter prediction model based on R-LSTM neural networks. The input complex-valued sequence is divided into real and imaginary parts and fed into the sea clutter prediction model. The obtained prediction results of real and imaginary parts are recombined into a complex number that is the corresponding predicted next time value of input complex-valued sequence.

optimized complex-valued neural networks model is proposed. The experimental results are demonstrated and analyzed in Section IV. Finally, Section V concludes this article.

II. Sea Clutter Prediction Model

The sea clutter sequences can be modeled as the output of a nonlinear chaotic dynamical system based on chaos theory [6]. According to Takens' embedding theorem [8], the system can be constructed into a predictive model so that sea clutter can be predicted accurately. A sea clutter sequence is denoted as $x(n), n = 1, 2, 3, \cdots, N$. With delay time τ and embedding dimension m [12], the single-variable time sequence can be reconstructed as follows:

$$\mathbf{X}(i, m) = \{x(i), x(i+\tau), \ldots, x(i+(m-1)\tau)\} \quad (1)$$

where $i = 1, 2, \ldots, N-(m-1)\tau$, and $\mathbf{X}(i, m)$ denotes the ith reconstructed vector with embedding dimension m. The estimation of τ and m directly affects the construction and prediction of the model, and the detailed estimation methods are introduced in Section III-B. The prediction equation is expressed as follows:

$$x(i+m\tau) = \mathrm{F}[\mathbf{X}(i, m)] \quad (2)$$

where F is a nonlinear mapping function. Therefore, the derivation of F is the major and most important part of the dynamical system reconstruction. Fortunately, neural networks are well suited to reconstructing nonlinear dynamics. Based on the abovementioned theory, Haykin and Li [6] proposed a one-step sea clutter prediction equation

$$x(i+m\tau) = \mathrm{G}[x(i), x(i+1), \ldots, x(i+m\tau-1)] \quad (3)$$

where $i = 1, 2, \ldots, N-m\tau+1$, and G is a nonlinear mapping function that reflects the evolution laws of the corresponding chaotic dynamic system. The input of (3) is expressed as $\mathbf{Y}(i) = \{x(i),\ x(i+1),\ \cdots,\ x(i+m\tau-1)\}$.

A. Classical Real-Valued Neural Networks Prediction Model

LSTM networks are capable of capturing the long-term temporal dependencies of input sequences. A sea clutter prediction model based on real-valued LSTM (R-LSTM) neural networks is trained to fit the nonlinear mapping function G in (3).

Since radar echo data are usually complex-valued data, real-valued networks cannot handle the complex-valued data directly. As shown in Fig. 1, the input complex-valued sequences are divided into real and imaginary parts and processed by the prediction model based on R-LSTM neural networks separately. Then, the obtained prediction results of the real and imaginary parts are recombined into a complex number, which is the predicted next time value of the input complex-valued sea clutter sequence. The training goal of the R-LSTM neural networks is to reduce the distance between the predicted result and ground truth. The loss functions of the R-LSTM neural networks for the real and imaginary parts are as follows:

$$\mathrm{Loss}_1 = \frac{1}{N}\sum_{i=1}^{N}(\mathbf{v}_i - \hat{\mathbf{v}}_i)^2 \quad (4)$$

$$\mathrm{Loss}_2 = \frac{1}{N}\sum_{i=1}^{N}(\mathbf{w}_i - \hat{\mathbf{w}}_i)^2 \quad (5)$$

where N is the number of training samples, $\mathbf{v}$ and $\mathbf{w}$ represent the real and the imaginary parts of the ground truth sea clutter, respectively, and $\hat{\mathbf{v}}$ and $\hat{\mathbf{w}}$ represent the real and the imaginary parts of predicted sea clutter, respectively.

B. Complex-Valued Neural Networks

For the aforementioned sea clutter prediction model based on R-LSTM neural networks, the input complex-valued sea clutter sequence is divided into real and imaginary parts and processed by the model separately, which discards the phase feature between the real and imaginary parts and damages the comprehensive features of complex-valued data. The motion of target produces noncooperative modulation to the phase of radar echo, and the phase of target signals need to be estimated. The phase of target signal is important for motion parameter estimation and imaging of moving ships. The lower the predicted phase error of sea clutter, the phase of target signals could be more accurate after sea clutter suppression. Therefore, the sea clutter models with low predicted phase error are required.

The real-valued neural network are extended to realize the processing of complex-valued sequences, which are called complex-valued neural networks. The process equations of complex-valued neural networks are introduced as follows:

$$\mathrm{f} = \mathrm{f}_1 + j\,\mathrm{f}_2 \quad (6)$$

$$\mathbf{z} = \mathbf{v} + j\,\mathbf{w} \quad (7)$$

where j is the imaginary unit ($j^2 = -1$), f represents the complex-valued neural networks, f_1 and f_2 represent a pair of real-valued neural networks, $\mathbf{z}$ is a complex-valued vector, and $\mathbf{v}$ and $\mathbf{w}$ are the real and imaginary parts of $\mathbf{z}$. The real and imaginary parts are computed in a similar manner via complex multiplication

$$\begin{aligned}\mathrm{f}(\mathbf{z}) &= (\mathrm{f}_1 + j\mathrm{f}_2) \otimes (\mathbf{v} + j\mathbf{w}) \\ &= [\mathrm{f}_1(\mathbf{v}) - \mathrm{f}_2(\mathbf{w})] + j[\mathrm{f}_2(\mathbf{v}) + \mathrm{f}_1(\mathbf{w})]. \end{aligned} \quad (8)$$

Fig. 2 shows the process of the complex-valued neural networks. The real and imaginary parts of the output complex-valued data are affected by the combination of the real and imaginary parts of the input complex-valued data. Compared with the real-valued neural networks, the complex-valued neural networks exist a connection between the real and imaginary parts through a mixed calculation.

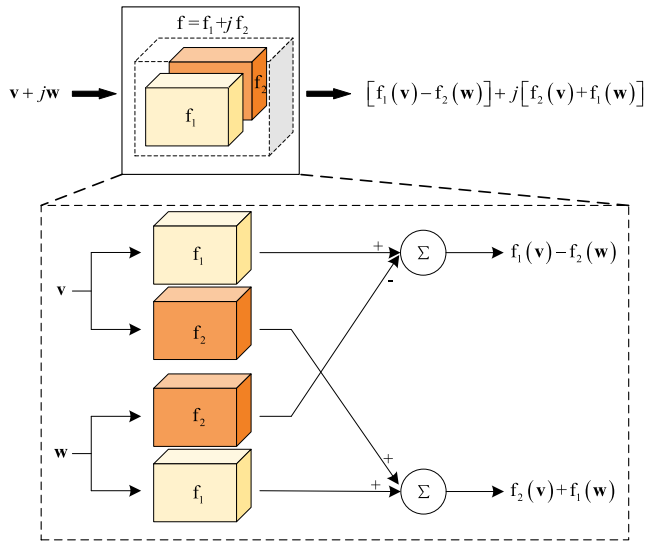

Fig. 2. Complex-valued neural networks. Two real-valued neural networks are integrated to realize phase processing.

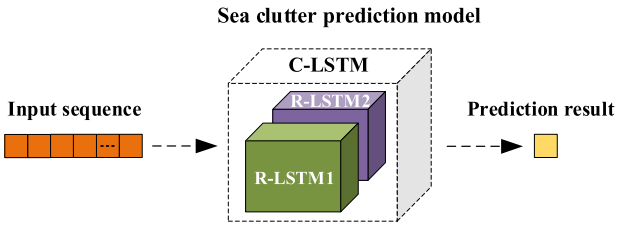

Fig. 3. Sea clutter prediction model based on C-LSTM neural networks. The input complex-valued sequence is fed into the sea clutter prediction model. The model outputs the obtained prediction result corresponding to the predicted next time value of the input complex-valued sequence.

The complex-valued sea clutter prediction model is shown in Fig. 3. In the architecture of the complex-valued LSTM (C-LSTM) neural networks, two R-LSTM neural networks are utilized to realize the processing of complex-valued data [16]. The model receives the complex-valued sea sequence and outputs a prediction result for the next time value of the input sequence.

The input of the C-LSTM neural networks is the complex-valued sea clutter sequence, which is regarded as 2-D data. The training goal of the C-LSTM neural networks is to reduce the distance between the predicted complex-valued sequence and the ground truth sea clutter sequence. The loss function is given as follows:

$$\mathrm{Loss}_3 = \frac{1}{2N}\sum_{i=1}^{N}\left[(\mathbf{v}_i - \hat{\mathbf{v}}_i)^2 + (\mathbf{w}_i - \hat{\mathbf{w}}_i)^2\right]. \tag{9}$$

The optimization problem for real-valued networks is a 1-D optimization problem. This kind of optimization method cannot obtain the optimal real and imaginary parts simultaneously. For the complex-valued networks, it is a 2-D joint optimization problem. The optimal real and imaginary parts are obtained simultaneously, and thus, the predicted phase error is decreased. Furthermore, the sea clutter prediction accuracy and the sea clutter suppression effect are improved.

C. Complex-Valued Neural Networks Optimized By PSD

During the training period, the complex-valued neural networks learn the inherent chaotic dynamical laws of the input sea clutter sequences. The neural networks attempt to capture the temporal dependencies of the input sequences. One of the important statistical characteristics of sea clutter is PSD [19], which represents the relationship between the signal power with the variation of the frequency. In essence, the autocorrelation function $\mathrm{R}_x(\tau)$ and the PSD $\mathrm{S}(f)$ are a pair of Fourier transforms

$$\mathrm{R}_x(\tau) = \sum_{n=1}^{N} x(n+\tau)\, x^*(n) \tag{10}$$

$$\mathrm{S}(f) = \mathcal{F}\left[\mathrm{R}_x(\tau)\right] \tag{11}$$

where $x^*(n)$ is the complex conjugate of $x(n)$, f denotes the frequency, and $\mathcal{F}$ denotes the Fourier transform. The PSD function is utilized to jointly optimize the complex-valued neural networks so that the networks could learn the sea clutter from the time domain and frequency domain. The joint optimization loss function is expressed as follows:

$$L = \alpha \mathrm{Loss}_3 + (1-\alpha)\frac{1}{2N-1}\sum_{f=1}^{2N-1}\left|S(f) - \hat{S}(f)\right|^2 \tag{12}$$

where L is the total loss, $S(f)$ and $\hat{S}(f)$ are the PSDs of the labeled data and the predicted data, respectively, and α is the loss weight that is assigned initial value of 0.5, and it is continually updated during the training of networks.

III. Sea Clutter Suppression Method

Based on the complex-valued neural networks, a sea clutter suppression method is proposed, as shown in Fig. 4. First, 1-D complex-valued sequences in each range cell of the range-compressed echo are normalized separately. Then the sea clutter component in the echo is estimated by applying the complex-valued sea clutter prediction model. Finally, the sea clutter suppression is realized by subtracting the estimated sea clutter from the original range-compressed echo.

A. Echo Normalization

In order to improve the convergence speed and accuracy of the prediction model, the radar echo data are normalized one by one for each range cell. For the complex-valued data, the normalization formula is

$$\mathbf{s}_{\mathrm{nor}} = \frac{\mathbf{s}}{\max\left(\mathrm{abs}\left(\mathbf{s}\right)\right)} \tag{13}$$

where $\mathbf{s}$ represents the complex-valued sea clutter sequence in each range cell, $\mathrm{abs}(\mathbf{s})$ represents the absolute value of $\mathbf{s}$, and $\max(\mathrm{abs}(\mathbf{s}))$ represents the maximum value of $\mathrm{abs}(\mathbf{s})$. After normalization, the absolute values of all the data are concentrated within the range of 0 to 1.

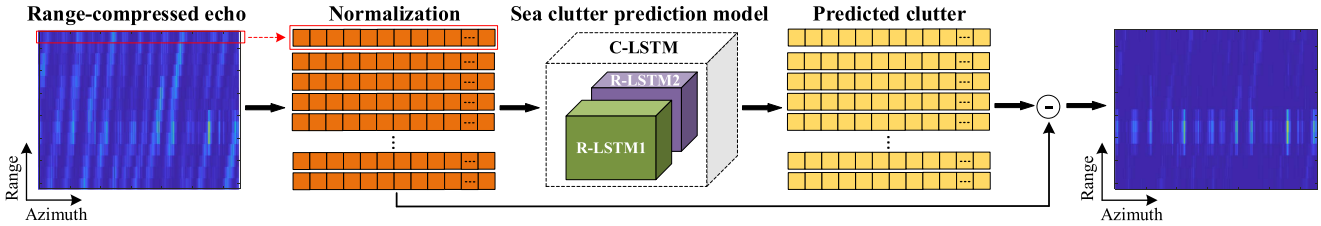

Fig. 4. Sea clutter suppression based on complex-valued sea clutter prediction model. The complex-valued sequences of the range-compressed echo are normalized by the range. Then, the sea clutter prediction model is applied and outputs the predicted result. Finally, the sea clutter suppression results are obtained by subtracting the predicted results from the original range-compressed echo.

B. Complex-Valued Model Training

The prediction model based on the complex-valued neural networks is trained to fit the nonlinear mapping function G in (3). First, the optimal delay time τ and the minimum embedding dimension m in the sea clutter prediction equation need to be estimated to ensure the dynamical characteristics of the sea clutter can be learned by the model.

1) Delay Time: The autocorrelation function $\mathrm{R}_x(\tau)$, defined in (10), is calculated to determine the optimal delay time τ. The time delay that makes the autocorrelation function value drop to $1-e^{-1}$ of its maximum value is optimal [8].

2) Minimum Embedding Dimension: The Cao algorithm is used to estimate the minimum embedding dimension m [20]. The minimum m is determined by the function $a(i,m)$, which is expressed as follows:

$$a\left(i,m\right)=\frac{\left\|\mathbf{X}\left(i,m+1\right)-\mathbf{X}\left(n\left(i,m\right),m+1\right)\right\|}{\left\|\mathbf{X}\left(i,m\right)-\mathbf{X}\left(n\left(i,m\right),m\right)\right\|} \tag{14}$$

where $\|\cdot\|$ is some measurement of the Euclidian distance. In this article, the following distance is used:

$$\left\|\mathbf{X}\left(k,m\right)-\mathbf{X}\left(l,m\right)\right\|=\max_{0\le s\le m-1}\left|x\left(k+s\tau\right)-x\left(l+s\tau\right)\right| \tag{15}$$

$\mathbf{X}(k,m)$ and $\mathbf{X}(l,m)$ represent the kth and lth reconstructed vectors with embedding dimension m, respectively, and $x(k+s\tau)$ and $x(l+s\tau)$ are the sth elements of the two reconstructed vectors. $n(i,m)$ $(1\le n(i,m)\le N-m\tau)$ is an integer that depends on i and m, and $\mathbf{X}(n(i,m),m)$ is the nearest neighbor of $\mathbf{X}(i,m)$ in the sense of the distance defined in (15). The mean value of all the $a(i,m)$ over i is as follows:

$$E\left(m\right)=\frac{1}{N-m\tau}\sum_{i=1}^{N-m\tau}a\left(i,m\right). \tag{16}$$

$E(m)$ depends on an embedding dimension m and delay time τ. $E_1(m)$ is utilized to investigate the variation of $E(m)$ from m to $m+1$ and is expressed as follows:

$$E_1\left(m\right)=\frac{E\left(m+1\right)}{E\left(m\right)}. \tag{17}$$

$E_1(m)$ does not vary significantly when m is greater than some value m_0. Then, m_0+1 is the minimum embedding dimension.

After the determination of τ and m, the training dataset can be constructed. As shown in Fig. 5, assuming the length of the complex-valued sequence is N, then $N-m\tau$ sequences with the length of $m\tau$ and the corresponding labels are obtained.

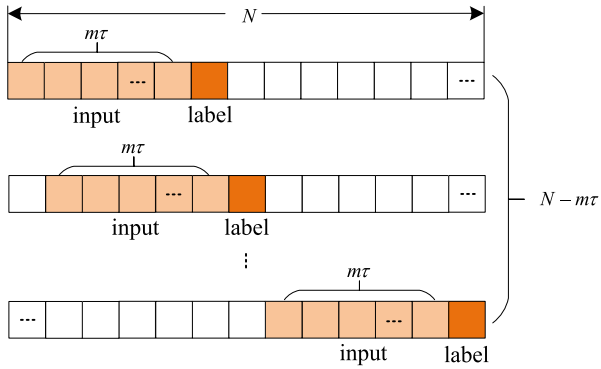

Fig. 5. Training dataset construction. A short sequence of length $m\tau$ is the input data of the model, and the next time value is the corresponding labeled data. Then, the starting point is moved to the right-hand side by one step, and the abovementioned steps are repeated until the end of the original sequence. For the original sequence of length N, $N-m\tau$ sets of inputs and corresponding labels are obtained.

C. Sea Clutter Estimation and Cancellation

The range-compressed echo in each range cell is input into the trained complex-valued prediction model to obtain the corresponding estimated sea clutter sequence. By cancellation, the estimated sea clutter is subtracted from the original range-compressed echo and the sea clutter suppression of radar echo is realized. If there exist targets in the echo, the target signals are left after sea clutter cancellation.

IV. Experimental Results and Analysis

The range-compressed radar echo provided by Naval Aeronautical University and the IPIX radar echo collected by the McMaster University of Canada were utilized to validate the proposed sea clutter suppression method [21], [22]. The prediction accuracy, sea clutter suppression performance, and signal-to-clutter ratio (SCR) improvements were analyzed.

A. Training Dataset

Three blocks of range-compressed echoes were selected: $\mathrm{Echo_A}$ and $\mathrm{Echo_B}$ were provided by Naval Aeronautical University, and their filenames were 20210106155330_01_staring

TABLE I
PARAMETERS OF RADAR ECHO

	Echo_A	Echo_B	Echo_C
Antenna polarization	HH	HH	VV
Azimuth angle (°)	42.18	8.01	170.26
Sea state	3–4	3–4	4
Radar frequency (GHz)	9.3–9.5	9.3–9.5	9.39
PRF (Hz)	3000	3000	1000
Pulse number	6940	4390	131072
Range cell number	4346	4346	14

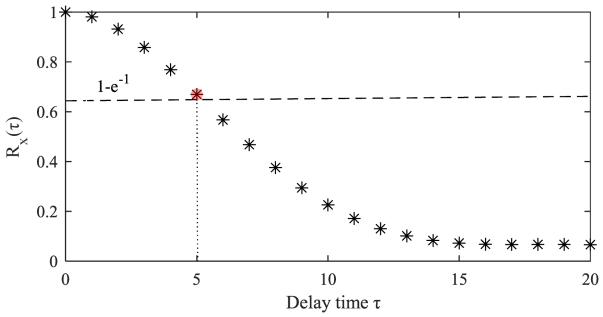

Fig. 6. Scatter diagram of the normalized autocorrelation function. When τ is 5, the autocorrelation value is closest to $1 - e^{-1}$.

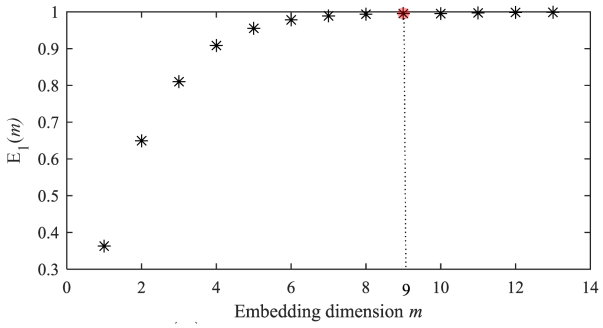

Fig. 7. Results of $E_1(m)$ with the increase in the embedding dimension m. $E_1(m)$ tended to be stable when m was greater than 9.

and 20210106172511_02_staring, respectively, and Echo_C was provided by the McMaster University of Canada, and its filename was 1931107_135603_starea. The parameters of the three blocks of echoes are given in Table I. Echo_A did not contain target signals. Both Echo_B and Echo_C contained target signals. The target signals in Echo_B mainly existed in the 940–953, 1482–1492, and 2140–2810 range cells. Echo_C contained a weak target signal in the 9th range cell and the adjacent 8th–11th range cells were affected by the target signal.

For each block of data, a range cell with a strong clutter energy and no target signal was selected to construct the training dataset, as shown in Fig. 5. The delay time τ and minimum embedding dimension m were estimated based on the autocorrelation function and the Cao algorithm introduced in Section III-B.

Fig. 6 shows the normalized autocorrelation function corresponding to the first range cell of Echo_A. The delay time $\tau = 5$ that made this function equal to $1 - e^{-1}$ was optimal. Fig. 7

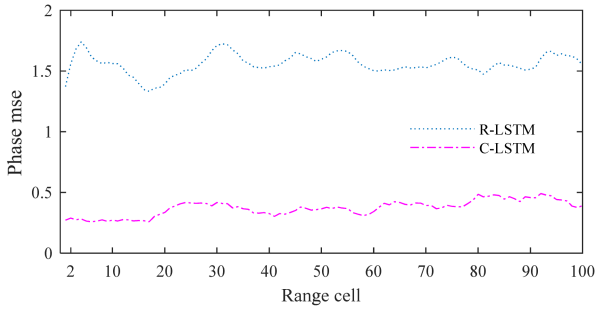

Fig. 8. Phase mse curves of Echo_A from the 2nd to the 100th range cell based on the R-LSTM model and the C-LSTM model.

shows the $E_1(m)$ obtained by applying the Cao algorithm. $E_1(m)$ tended to be stable after $m = 9$. Thus, the minimum embedding dimension $m = 10$. The signal length in one range cell of Echo_A was 6940. Thus, 6890 sequences with the lengths of 50 were obtained to construct the training dataset. Similarly, τ and m were 3 and 14, respectively, for Echo_B. For Echo_C, τ and m were 5 and 12, respectively.

The number of layers of the C-LSTM networks, the number of hidden nodes, the batch size, the learning rate, and the number of training iterations were set to 2, 32, 64, 0.0002, and 25, respectively. As introduced in Section II-C, the data loss function and the PSD loss function were utilized to jointly optimize the complex-valued neural networks. The Adam algorithm was used to optimize parameters during the training.

B. Prediction Accuracy of Sea Clutter

The ground truth of the sea clutter component is difficult to obtain in an echo that contains sea clutter and target signals. Echo_A described in Section IV-A did not contain target signals and was considered to be sea clutter data. Thus, Echo_A was utilized in the phase evaluation experiment. The phase mean square error (mse) of each range cell was determined as follows:

$$\text{phase mse} = \frac{1}{N}\sum_{i=1}^{N}\left(\text{phase}\left[x\left(i\right)\right] - \text{phase}\left[\hat{x}\left(i\right)\right]\right)^2 \tag{18}$$

where N is the number of sampling points in the azimuth, and $x(i)$ and $\hat{x}(i)$ are the original complex-valued sea clutter data and the predicted data, respectively. phase$[x(i)]$ represents the phase value of $x(i)$ and is determined by

$$\text{phase}\left[x\left(i\right)\right] = \arctan\left\{\frac{\text{imag}\left[x\left(i\right)\right]}{\text{real}\left[x\left(i\right)\right]}\right\} \tag{19}$$

where arctan is the arctangent function, and real$[x(i)]$ and imag$[x(i)]$ are the real and imaginary parts of $x(i)$, respectively. Fig. 8 shows the phase mse curves of Echo_A from the 2nd to the 100th range cell based on the R-LSTM model and the C-LSTM model. The phase mse of the C-LSTM was smaller than that of the R-LSTM.

The coefficient of determination (R-squared) is an evaluation index that measures the quality of the fit of model. It was applied

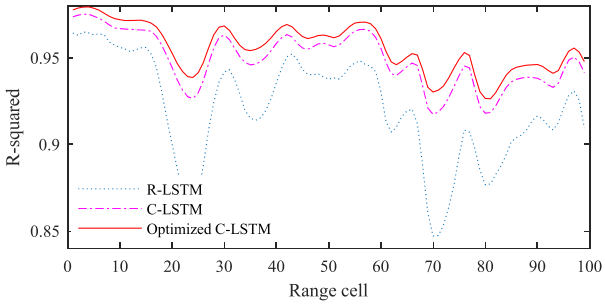

Fig. 9. R-squared curves obtained by processing Echo_A from the 2nd to the 100th range cell based on R-LSTM, C-LSTM, and optimized C-LSTM models.

to evaluate the prediction accuracy, and is defined as follows:

$$\text{R-squared} = 1 - \frac{\sum_{i=1}^{n} (x_i - \hat{x}_i)^2}{\sum_{i=1}^{n} (x_i - \bar{x})^2} \tag{20}$$

where n is the number of training samples, x_i represents the ground truth, $\hat{x}_i$ is the prediction result, and $\bar{x}$ is the mean value of x. The closer R-squared is to 1, the better the similarity between the prediction results and the ground truth is, and the higher the prediction accuracy is. Fig. 9 shows the R-squared curves obtained by processing Echo_A from the 2nd to the 100th range cell based on the R-LSTM model, C-LSTM model, and C-LSTM model optimized by the PSD (henceforth referred to as optimized C-LSTM model). The prediction accuracy achieved by the C-LSTM model improved significantly compared with that of the R-LSTM model. With the inclusion of the PSD, the optimized C-LSTM model further improved the prediction accuracy for the sea clutter. The average R-squared coefficients achieved by the R-LSTM, C-LSTM, and optimized C-LSTM models were 0.9213, 0.9492, and 0.9561.

C. SCR Improvement

Fig. 10 shows the sea clutter suppression results for Echo_A, which contained no targets. Fig. 10(a)–(c) compare the original echo in the 40th range cell with the sea clutter suppression results obtained by the R-LSTM, C-LSTM, and optimized C-LSTM models, respectively. The energy of the sea clutter was suppressed by 10.36, 12.53, and 13.20 dB on average for these three models, respectively. Fig. 10(d) compares the resulting normalized profiles of the 43rd pulse from the 2nd to the 100th range cell, which also indicated that the optimized C-LSTM model was superior to the other two models in sea clutter suppression.

Fig. 11 illustrates the sea clutter suppression results for Echo_B. Fig. 11(a)–(c) compare the results in the 945th range cell achieved by the three models. The resulting normalized profiles corresponding to the 43rd pulse from the 701st to the 1200th range cell are compared in Fig. 11(d). R-LSTM, C-LSTM, and optimized C-LSTM models improved the SCR by 3.83, 5.34, and 6.33 dB, respectively.

Fig. 12 shows the sea clutter suppression results for Echo_C. The resulting profiles corresponding to the 69 869th pulse from the 1st to the 14th range cell obtained by the C-LSTM model

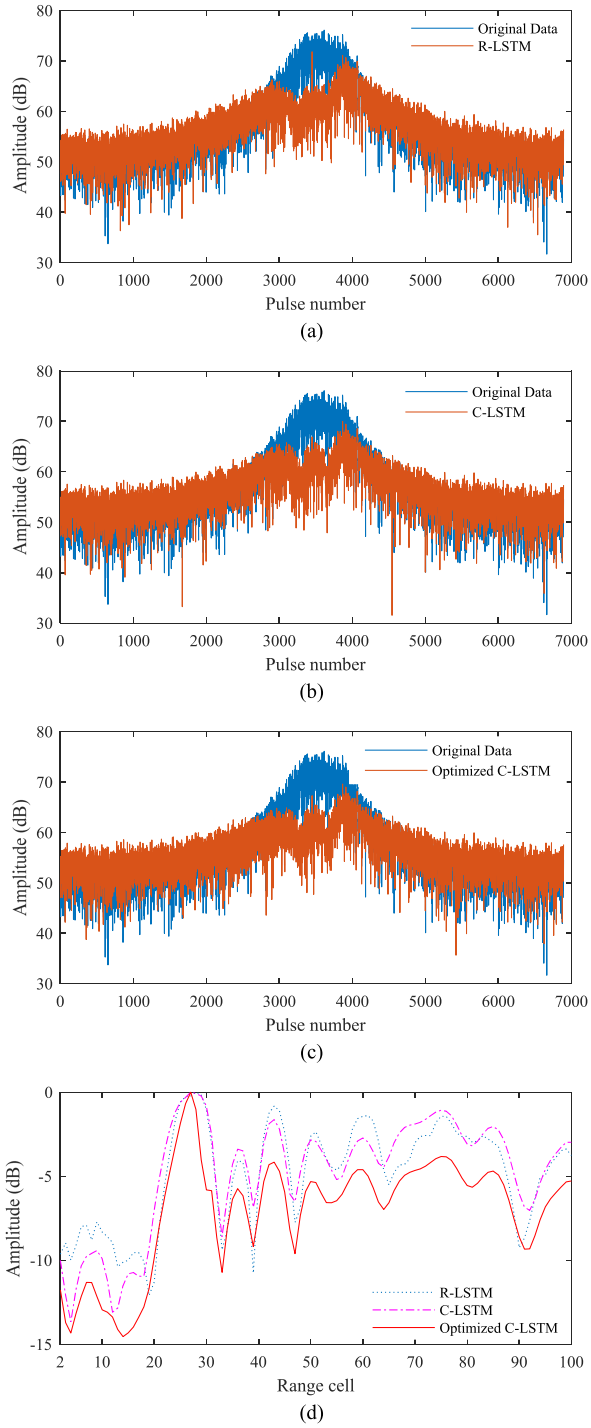

Fig. 10. Sea clutter suppression results for Echo_A. Comparison between the original echo in the 40th range cell with the results obtained by the (a) R-LSTM, (b) C-LSTM, and (c) Optimized C-LSTM models. (d) Normalized resulting profiles of the 43rd pulse from the 2nd to the 100th range cell obtained by the three models.

and the optimized C-LSTM model are compared in Fig. 12(a). The proposed optimized C-LSTM model not only suppressed the sea clutter, but also better maintained the target signal. The R-LSTM, C-LSTM, and optimized C-LSTM models improved the SCR by 1.54, 12.35, and 14.91 dB, respectively. Fig. 12(b) and (c) shows the images of Echo_C and the imaging result.

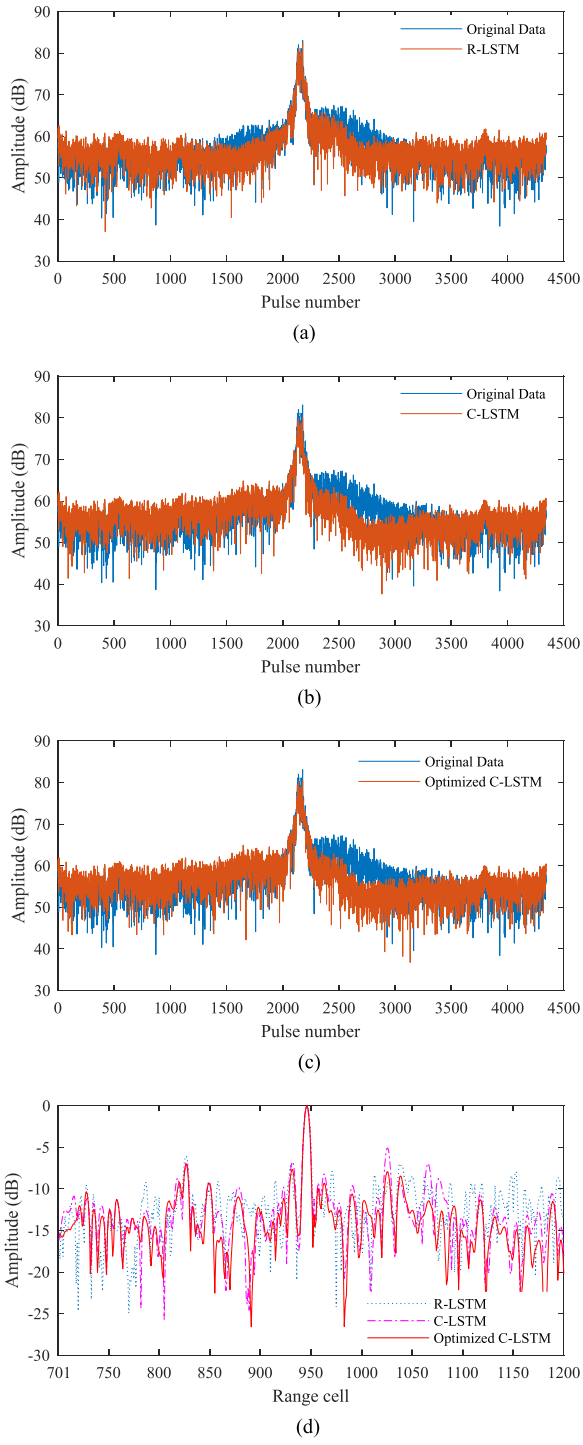

Fig. 11. Sea clutter suppression results for Echo_B. Comparison between the original echo in the 945th range cell with the results obtained by the (a) R-LSTM, (b) C-LSTM, and (c) optimized C-LSTM models. (d) Normalized resulting profiles of the 43rd pulse from the 701st to the 1200th range cell obtained by the three models.

Fig. 12(d) and (e) shows the suppression results of Echo_C and the corresponding imaging result based on the optimized C-LSTM model. Based on the abovementioned results and analysis, the proposed C-LSTM model optimized by the PSD exhibited an excellent sea clutter suppression performance.

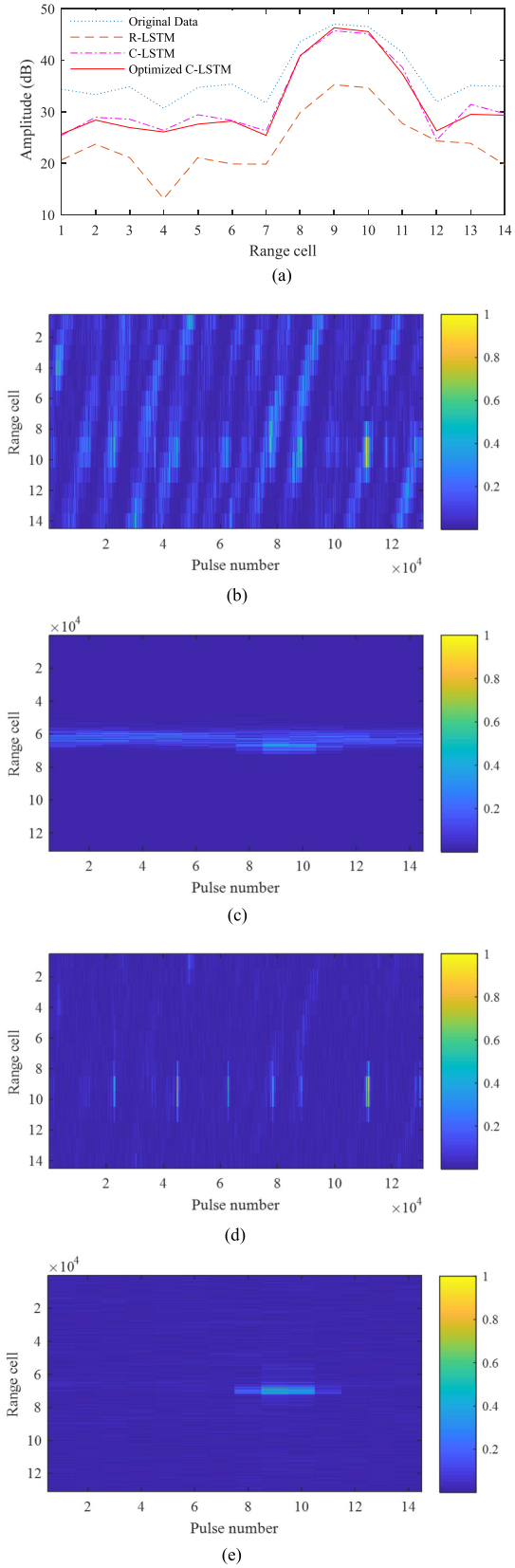

Fig. 12. Sea clutter suppression results for Echo_C. (a) Resulting profiles of the 69 869th pulse from the 1st to the 14th range cell obtained by R-LSTM, C-LSTM, and optimized C-LSTM models. (b) Echo_C. (c) Imaging result of Echo_C. (d) Sea clutter suppressed Echo_C based on the optimized C-LSTM model. Sea clutter suppression results for Echo_C. (e) Imaging result of (d).

V. Conclusion

Based on a chaotic prediction model, a new sea clutter suppression method based on a complex-valued neural networks optimized by the PSD is proposed in this article. The validation results of the measured sea clutter data showed that the proposed method achieved better results on sea clutter prediction and suppression than the R-LSTM model and C-LSTM model. In the future, we will try to integrate sea clutter suppression and motion parameter estimation to improve the image focusing performances for moving ships.

References

[1] J. Yu, Z. Yu, and C. Li, "GEO SAR imaging of maneuvering ships based on Time–frequency features extraction," *IEEE Trans. Geosci. Remote Sens.*, vol. 60, Apr. 2022, Art. no. 5226321, doi: 10.1109/TGRS.2022.3166758.

[2] Z. W. Guan, J. W. Chen, and B. Zheng, "Modified method of sea clutter cancellation for sky wave radar," *J. Air Force Early Warning Acad.*, vol. 28, no. 5, pp. 318–322, 2014.

[3] F. Jangal, S. Saillant, and M. Helier, "Wavelet contribution to remote sensing of the sea and target detection for a high-frequency surface wave radar," *IEEE Geosci. Remote Sens. Lett.*, vol. 5, no. 3, pp. 552–556, Jul. 2008.

[4] G. Wang et al., "Manoeuvring target detection in over-the-horizon radar using adaptive clutter rejection and adaptive chirplet transform," *IEE Proc. Radar Sonar Navigation*, vol. 150, no. 4, pp. 292–298, May 2003.

[5] M. W. Y. Poon, R. H. Khan, and S. Le-Ngoc, "A singular value decomposition (SVD) based method for suppressing ocean clutter in high frequency radar," *IEEE Trans. Signal Process.*, vol. 41, no. 3, pp. 1421–1425, Mar. 1993.

[6] S. Haykin and X. B. Li, "Detection of signals in chaos," *Proc. IEEE*, vol. 83, no. 1, pp. 95–122, Jan. 1995.

[7] T. Matsumoto, Y. Nakajima, M. Saito, J. Sugi, and H. Hamagishi, "Reconstructions and predictions of nonlinear dynamical systems: A hierarchical Bayesian approach," *IEEE Trans. Signal Process.*, vol. 49, no. 9, pp. 2138–2155, Sep. 2001.

[8] F. Takens, "Detecting strange attractors in turbulence," in *Lecture Notes in Mathematics*, J. M. Morel and B. Teissier, Eds. Cham, Switzerland: Springer, 1981, pp. 366–381.

[9] S. Xiaohong and S. Jidong, "Prediction of sea clutter based on chaos theory with RBF and K-mean clustering," in *Proc. CIE Int. Conf. Radar*, 2006, pp. 1–4.

[10] B. Zhou and A. Shi, "Application of wavelet neural network for chaos time series prediction," in *Proc. 5th Int. Conf. Intell. Hum. Mach. Syst. Cybern.*, 2013, pp. 259–262.

[11] Z. Gao and L. Chen, "Sea clutter sequences regression prediction based on PSO-GRNN method," in *Proc. 8th Int. Symp. Compu. Intel. Des.*, 2015, pp. 72–75.

[12] L. W. Ma et al., "Sea clutter amplitude prediction using a long short-term memory neural network," *Remote Sens.,* vol. 11, no. 23, Dec. 2019, Art. no. 2826.

[13] S. Shang et al., "Sea clutter suppression method of HFSWR based on RBF neural network model optimized by improved GWO algorithm," *Comput. Intell. Neurosci.,* vol. 2020, 2020, Art. no. 842390.

[14] C. Trabelsi et al., "Deep complex networks," in *Proc. Int. Conf. Learn. Representations*, Feb. 2018, pp. 1–19.

[15] I. Danihelka et al., "Associative long short-term memory," in *Proc. 33rd Int. Conf. Mach. Learn.*, 2016, pp. 1986–1994.

[16] R. G. Goswami et al., "Phase aware speech enhancement using realisation of Complex-valued LSTM," Oct. 2020. [Online] Available: https://arxiv.org/pdf/2010.14122.pdf

[17] J. Gao, B. Deng, Y. Qin, H. Wang, and X. Li, "Enhanced radar imaging using a complex-valued convolutional neural network," *IEEE Geosci. Remote Sens. Lett.*, vol. 16, no. 1, pp. 35–39, Jan. 2019.

[18] A. Hirose and S. Yoshida, "Generalization characteristics of complex-valued feedforward neural networks in relation to signal coherence," *IEEE Trans. Neural Netw. Learn. Syst.*, vol. 23, no. 4, pp. 541–551, Apr. 2012.

[19] M. Demiański, A. G. Doroshkevich, and V. Turchaninov, "Statistical characteristics of the observed Ly α forest and the shape of initial power spectrum," *Monthly Notices Roy. Astronomical Soc.*, vol. 340, no. 2, pp. 525–542, Apr. 2003.

[20] L. Cao, "Practical method for determining the minimum embedding dimension of a scalar time series," *Phys. Rev.*, vol. 110, pp. 43–50, May 1997.

[21] N.B. Liu et al., "Annual progress of Sea-detecting X-band radar and data acquisition program," *J. Radars*, vol. 10, no. 1, pp. 173–182, Feb. 2021.

[22] S. Haykin, C. Krasnor, T. J. Nohara, B. W. Currie, and D. Hamburger, "A coherent dual-polarized radar for studying the ocean environment," *IEEE Trans. Geosci. Remote Sens.*, vol. 29, no. 1, pp. 189–191, Jan. 1991.

Hongling Zhu was born in Yichun, Jiangxi, China, in 1998. She received the B.S. degree in communication engineering from Central South University, Changsha, Hunan, China, in 2020. She is currently working toward the M.A. Eng. degree in signal and information processing from Beihang University, Beijing, China.

Her research interests include the application of deep learning in remote sensing, clutter suppression, and imaging processing for synthetic aperture radar.

Ze Yu (Member, IEEE) was born in Xi'an, Shaanxi, China, in 1979. He received the B.S. degree in electronics engineering and the Ph.D. degree in communication and information system from Beihang University, Beijing, China, in 2002 and 2007, respectively.

Since 2009, he has been with the School of Electronics and Information Engineering, Beihang University. He is currently involved in the system design and imaging processing for high-resolution and wide-swath synthetic aperture radar.

Jindong Yu was born in Tianjin, China, in 1992. He received the B.S. degree in electronics engineering and the Ph.D. degree in signal and information processing from Beihang University, Beijing, China, in 2015 and 2022, respectively.

Since 2022, he has been a Postdoc with the School of Electronics and Information Engineering, Beihang University. His research interests include system analysis and imaging processing for synthetic aperture radar moving target.